

paces: Parallelized Application of Co-Evolving Subspaces, a method for computing quantum dynamics on GPUs

R. Kevin Kessing

¹*Institut für Theoretische Physik, Universität Ulm, 89069 Ulm, Germany*

²*Institut für Theoretische Physik, Georg-August-Universität Göttingen, 37077 Göttingen, Germany*

³*Department of Chemistry, Massachusetts Institute of Technology, Cambridge, Massachusetts 02139*

(*Electronic mail: kevin.kessing@uni-ulm.de)

An efficient method of computing the dynamics of a pure quantum state under the time-dependent Schrödinger equation is described: At each timestep, a restricted subspace of the potentially infinite-dimensional total Hilbert space is systematically and naturally constructed via the image of repeated applications of the Hamiltonian operator, and the time evolution is computed exactly within said subspace. The subspace is dynamically recomputed at each timestep such that it co-evolves with the state vector. We benchmark the method using the Holstein model and compare the formal information content of its representation to the matrix-product state formalism. The method is built from the ground up as a parallel algorithm for graphics processing units and is applicable to arbitrary Hamiltonians that are sparse in a given basis. It can be extended to open quantum system dynamics and/or time-dependent generators.

I. INTRODUCTION & MOTIVATION

The dynamics of any closed quantum system are given by the time-dependent Schrödinger equation (TDSE),

$$i\hbar \frac{\partial}{\partial t} |\psi(t)\rangle = H |\psi(t)\rangle,$$

whose solution is formally—if the Hamiltonian operator H is time-independent—given by

$$|\psi(t)\rangle = e^{-itH/\hbar} |\psi(0)\rangle, \quad (1)$$

where $|\psi(0)\rangle$ is the initial state which we want to evolve in time and $|\psi(t)\rangle$ is the state after evolving for some time t . In practice, equation 1 usually cannot be computed exactly due to the well-known “curse of (exponential) dimensionality”^{1–4}, i.e., the exponential growth of the Hilbert space with respect to the system size, which prohibits a complete analysis of all but the simplest problems (e.g., a laser-driven H_2 molecule⁵). Therefore, a number of approaches have been developed that effectively try to reduce the size of the problem to a manageable scale. In this article, we present a highly-parallelizable method of solving the TDSE based on adaptive or “co-evolving” subspaces that is fully implementable on graphics processing units (GPUs). This method has been successfully applied in a previous publication⁶, but the present publication constitutes the first detailed explanation and investigation of its strengths and weaknesses.

This paper is structured as follows: In section I, we sketch the main concepts of three groups of existing methods for computing quantum dynamics and outline their differences or similarities to the present method. Section II provides a high-level overview of the idea of the method, which is explained in further detail—also with regards to implementation details surrounding parallelizability—in section III. In section IV, we compare the information content of the sparse or truncated

vector representation adopted here to the information content of an identical state written as a matrix product state. Section V is concerned with error analysis and benchmarking, and we conclude by discussing the method’s future expandability in the final section VI.

A. Sketch of existing methods

A family of very widespread methods in modern computational physics are matrix-product state (MPS) approaches, which built on earlier density-matrix renormalization group (DMRG)^{7–9} and numerical renormalization group concepts¹⁰. We briefly present the core ideas behind these methods here and anticipate how they compare to the present method. See, e.g., refs. 11–13 for more detailed modern reviews of these methods.

MPS methods deal with the curse of dimensionality by locally decomposing and compressing vectors and operators: In a d^L -dimensional Hilbert space consisting of L sites (each with a local dimension d), an arbitrary state vector $|\psi\rangle$

$$|\psi\rangle = \sum_{\sigma_1, \dots, \sigma_L} \psi_{\sigma_1, \dots, \sigma_L} |\sigma_1, \dots, \sigma_L\rangle,$$

where $\psi_{\sigma_1, \dots, \sigma_L}$ are the typical state vector coefficients, can be rewritten as

$$|\psi\rangle = \sum_{\sigma_1, \dots, \sigma_L} A_{\sigma_1}^{(1)} \cdots A_{\sigma_L}^{(L)} |\sigma_1, \dots, \sigma_L\rangle$$

by repeatedly reshaping $\psi_{\sigma_1, \dots, \sigma_L}$ and applying Schmidt decompositions to the resulting matrices. Each of the $A_{\sigma_i}^{(i)}$ in this equation is a matrix, and since there are d matrices associated to each site (each matrix corresponding to a different local basis state σ_i), each $A^{(i)}$ constitutes a third-order tensor.

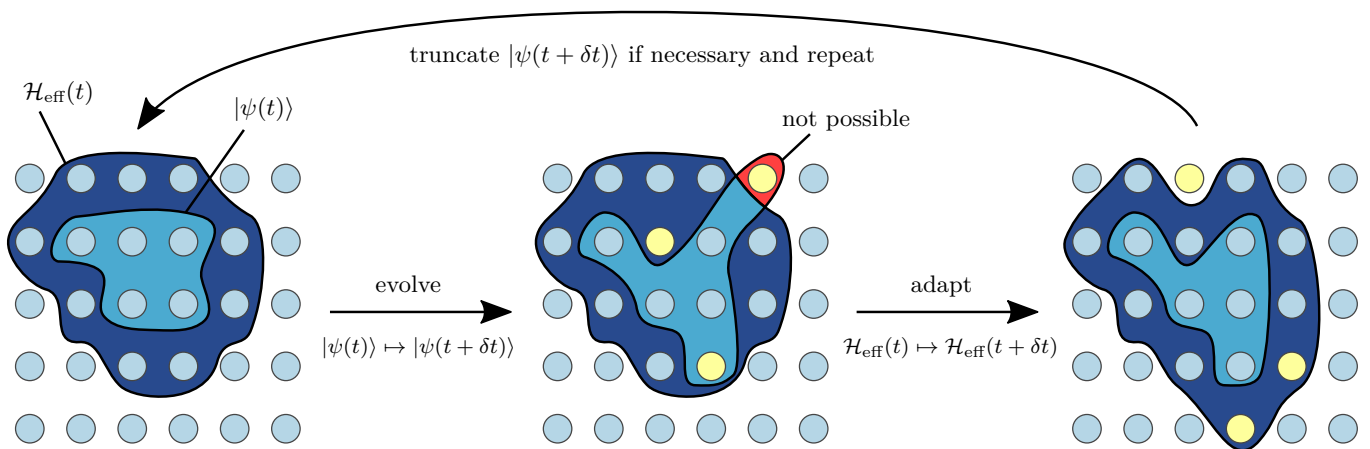


FIG. 1. The basic idea of *paces*: Construct an effective Hilbert space, evolve exactly within this effective Hilbert space, truncate and repeat. Each circle represents a basis state. Dark blue: the effective Hilbert subspace; light blue: non-zero components of the state vector; yellow highlighting: basis states affected by a change.

The two main merits of the MPS approach are that there is now a physically motivated local decomposition which may ease calculations, and that there is a natural way to compress such a decomposed state by applying singular value decompositions (SVD) to each $A^{(i)}$ and truncating the lowest-weight singular values such that only χ_{\max} singular values are retained. χ_{\max} is then called the *bond dimension*. The truncated $A_{\sigma_i}^{(i)}$ are then matrices of dimensions less than or equal to $\chi_{\max} \times \chi_{\max}$. Physically, this truncation of the matrices corresponds to truncating the entanglement between lattice sites. Because of this, combined with the area law of entanglement, certain geometrically low-dimensional Hamiltonians are known to admit highly efficient MPS representations¹⁴. However, general systems, especially highly interconnected or (geometrically) higher-dimensional ones, generally do not exhibit such “nice” properties and may suffer significantly from the entanglement-based truncation: Intuitively, we see that the MPS decomposition given above requires a natural one-dimensional ordering, since any given tensor $A^{(i)}$ must contract only with its “neighboring” tensors $A^{(i-1)}$ and $A^{(i+1)}$; thus, if a system does not exhibit such a 1D order, apparent long-range correlations and entanglement may arise from forcing a 1D ordering onto the system, inhibiting the compression and complicating the computation of such a system^{15,16}. As we demonstrate below, the present method does not impose such a 1D ordering on the system and is therefore geometry-agnostic, eliminating the need for optimized “topologies” of local sites.

As described above, the standard SVD-based compression used for MPS effectively truncates the inter-site entanglement, but it does not affect the—potentially very large—local dimension d of the state being described by an MPS. Therefore, further techniques have been developed to efficiently truncate the local dimension d in MPS, in particular, the procedure that later became known as local basis optimization (LBO)^{17–20}. The basic idea be-

hind LBO is to diagonalize the reduced density matrix at each site and then retain only those eigenvectors of the reduced density matrix that correspond to the largest eigenvalues, based on some cutoff weight, similar to the truncation procedure used in our method (section III C).

There is another, separate class of methods which the present method closely resembles and which originated mostly in theoretical chemistry: methods of adaptive basis sets. These methods deal with the exponential growth of the Hilbert space by choosing a small, truncated Hilbert space and systematically adapting the basis set to the evolution of the state vector. Most of these methods employ a basis of time-dependent Gaussian wavepackets (GWPs) which move to follow the current state based on, e.g., classical/Ehrenfest dynamics (e.g.,^{21–25}) or quantum hydrodynamic trajectories^{26,27}, by periodically re-expanding the wavefunction in a new Gaussian basis^{28–32}, or by employing a set of GWP basis states variationally³³. Though the use of approximate trajectories to optimize basis set can be beneficial, it requires devoting computational resources to the calculation of said trajectories and can potentially lead to issues surrounding the non-orthogonality/over-completeness of Gaussian basis sets. We point out that one family of methods known as *wavepacket propagation in a distributed Gaussian basis* (PRODG)^{34,35} is, however, particularly similar to the present method, as uses a fixed total set of basis states and adaptively adds or remove basis states to or from the current basis set depending on the weight of the wavefunction on that particular basis set.

A fundamental difference between most of these methods (a partial exception being the orthogonalized “interpolating Gaussians” of 35) and ours is that we employ a countable orthogonal underlying basis set that is not over-complete. Whether such a more countable and orthogonal basis set may be reasonably chosen depends on the system in question, though we point out that the Fock basis may be used for a wide variety of systems of

interest to physics and chemistry, and fermionic systems often feature a canonical countable basis. Which basis delivers superior performance in practice is not necessarily clear a priori and will depend on the situation at hand, and will depend in particular on the representation of the Hamiltonian matrix and the initial state in the given basis.

Finally, though it was not originally developed from the limited functional space (LFS) method developed by Bonča et al.³⁶ and applied in many subsequent publications^{37–46}, the present method can essentially be viewed as a generalization of the LFS method. LFS uses the same method of adding basis states via the image of the Hamiltonian as described in section III B 2. However, to the best of our knowledge—using the terminology of the present method—all past approaches have constructed the “effective” Hilbert space only a single time and our method is the first to instead adaptively reconstruct it in a “co-evolving” manner. Furthermore, we designed our method from the ground up to be as parallelizable as possible, such that it particularly suited to parallel implementation on GPUs.

II. THE ESSENCE OF PACES: FOLLOWING A WAVEFUNCTION AS IT PROPAGATES

The basic idea of the present method is to efficiently truncate the high-dimensional Hilbert space to a smaller Hilbert space in a time-dependent manner, similar to the core idea behind time-dependent DMRG^{13,47}. However, unlike the SVD-based compression of MPS methods, the present method uses a different expansion-and-truncation technique to manage the effective Hilbert space.

The basic idea can be described as follows (illustrated in Fig. 1): In a finite-dimensional Hilbert space \mathcal{H} spanned by a countable orthonormal basis \mathfrak{B} , assume our initial state vector $|\psi\rangle$ has non-zero basis coefficients $\psi_n = \langle n|\psi\rangle$ for only a small number of basis states $|n\rangle \in \mathfrak{B}$. Then:

1. *construct* a Hilbert subspace, called the *effective Hilbert space* $\mathcal{H}_{\text{eff}}(t)$, of the entire \mathcal{H} ; this Hilbert subspace should capture both the current state vector and “neighboring” basis states into which the state vector may evolve,
2. then construct the Hamiltonian matrix acting on this Hilbert subspace and *evolve* the state vector based on the Hamiltonian within the subspace (using $U = e^{-iH\delta t/\hbar}$),
3. and finally, if necessary, *truncate* the resulting state vector so as to prevent a memory overflow in the following iteration, and repeat from step 1.

The notion of a “neighboring” basis state defined generically in terms of the image of the Hamiltonian acting on the state at a time t , as explained below.

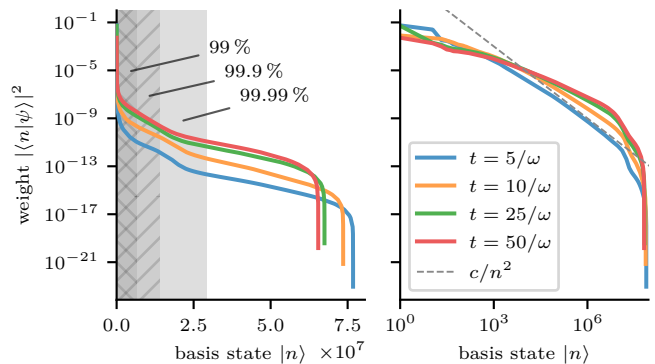


FIG. 2. The distribution of the expansion coefficients for a *paces* Holstein model at several times after the start of the evolution from a fully localized Franck–Condon excitation, in a lin-log plot (left) and a log-log plot (right). We see that the vast majority of basis states contribute negligibly to the total wavefunction, and the distribution (for the most part) seems to be in between an exponential and a power law, spreading out over time. The hatched areas apply to the fat-tailed $t = 50/\omega$ state and show that less than half of the coefficients account for 99.99% of the total weight. The dashed line shows a $1/n^2$ power law that is speculated to be attained here (see section V B). Parameters: $L = 25$, $g = 4\hbar\omega$, $J = \hbar\omega$.

Note that all three steps are repeated at every timestep, such that the effective subspace is reconstructed at every timestep, hence our designation “co-evolving subspaces”. Furthermore, the present method was designed from the ground up for parallelized deployment on GPUs, hence the designation “parallelized co-evolving subspaces” or *paces*.

The motivation for the recurring and adaptive recalculation of the relevant Hilbert subspace is that most of a Hilbert space is irrelevant to finite-time dynamics^{48,49}: Given an initial state in an exponentially or infinitely large spin system Hilbert space, then given any realistically scaled Hamiltonian, the time it would take to evolve into most parts of the Hilbert space would far exceed the relevant timescales, such that only an exponentially tiny fraction of the Hilbert space is relevant for finite-time evolution. This concept is visualized in Fig. 2, which shows the highly localized distribution of the coefficients $|\langle n|\psi\rangle|^2$ in a post-quench Holstein model (3) as an example. Assuming the distribution of the coefficients is exponential, then by keeping only n basis states and neglecting the remaining, potentially infinitely many, $(\dim \mathcal{H} - n)$ basis states, we would incur an error only of order $\mathcal{O}(e^{-\lambda n})$. As another, simpler example, if we consider the time evolution of a linearly displaced harmonic oscillator, i.e., a system described by a Hamiltonian of the type

$$H = \hbar\omega a^\dagger a + \hbar\lambda (a + a^\dagger),$$

from an initial vacuum state $|\psi(0)\rangle = |0\rangle$, we get a time evolution as in Fig. 3. We see that most of the Hilbert space is irrelevant to the time evolution at any given time

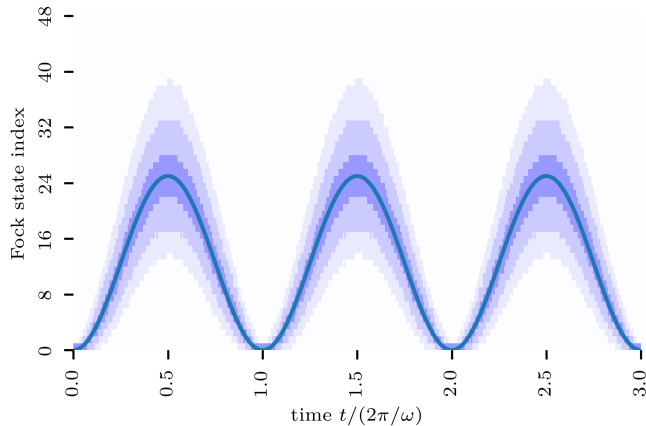


FIG. 3. The time evolution of a perturbed quantum harmonic oscillator (QHO), $H = (\hbar\omega) [a^\dagger a + 2.5(a + a^\dagger)]$, starting from an initial vacuum state $|0\rangle$. The dark blue line is the average occupation number, and the shaded areas mark the basis states required to capture 50%, 90% or 99% of the weights $|\langle n|\psi(t)\rangle|^2$ of the state.

and that a relatively small set of basis states suffices to describe the majority of the state at any time, but that the set of relevant basis states change (or, in this case, oscillates) over time. Thus, at any time, we could imagine following the state in its time evolution with only 10 or 20 basis states and capture essentially the entire dynamics by neglecting all the basis states outside of these basis states, thereby saving enormous computational resources by not even constructing the irrelevant parts of the Hamiltonian, state vector, etc.

If the underlying \mathcal{H} is infinite-dimensional, a finite-dimensional subspace \mathcal{H}' must be chosen for the computation. However, the dimension of this restricted subspace can be chosen to be very large: If a well-suited basis is chosen, then most basis states of \mathcal{H} are not explored in finite time and the effect of the cutoff dimension is mostly restricted to a lookup table that connects the truncated state vector with its physical index. As a function of the total dimension $d_{\text{tot}} = \dim \mathcal{H}'$, the memory required by this lookup table grows as $\mathcal{O}(\log_2 d_{\text{tot}})$.

As is visualized in Fig. 1, such an adapted Hilbert subspace restricts the possible “movement” or propagation of the state vector at each timestep. Though the time evolution can be performed to an essentially exact degree within the effective Hilbert space, the timestep δt must be chosen small enough so that the restriction to the effective subspace does not skew the results. A greater problem that can arise is diffusion-like propagation or spreading of wavefunctions in a given basis: Contrast the coherent behavior of a simple system such as the harmonic oscillator shown in Fig. 3 with the increasing spread of the wavefunction coefficients over time shown in the Holstein model in Fig. 2. At some point, even though the truncated Hilbert space is sufficiently small for each given timestep, the entire state vector may blow up to a

degree that exceeds the available memory, such that the entire state can no longer be accurately represented at some point in time.

III. DETAILS OF PACES

We shall now present the building blocks that form the foundation of the *paces* method.

As an example system, we will, in the following, refer to the 1D single-exciton tight-binding (TB) Hamiltonian H_{TB} with open boundary conditions,

$$H_{\text{TB}} = \sum_{k=1}^L \epsilon_k |k\rangle\langle k| + \left[\sum_{k=1}^{L-1} J_k |k\rangle\langle k+1| + \text{h.c.} \right] \quad (2)$$

and the Holstein Hamiltonian, which is based on the TB Hamiltonian:

$$H_{\text{H}} = H_{\text{TB}} + \sum_{k=1}^L [\hbar\omega_k a_k^\dagger a_k + \hbar g_k |k\rangle\langle k| (a_k^\dagger + a_k)], \quad (3)$$

where a_k is the annihilation operator of the k -th quantum harmonic oscillator (QHO), representing a phononic mode at site k , and $|k\rangle$ is the excitonic wavefunction when the exciton is fully localized to the k -th site. ω_k , ϵ_k , g_k and J_k are the k -th phonon frequency, local exciton energy, exciton–phonon coupling and excitonic hopping strength (nearest-neighbor dipole–dipole coupling), respectively. In the following, the parameters are often identical for each site, in which case we will drop the index k . Note that due to the restriction to the single-exciton manifold, the model can also be interpreted as a single-electron model without further loss of generality.

A. The time evolution step using a sparse Hamiltonian

Most Hamiltonians encountered in condensed-matter physics, when written in a “reasonable” basis, are sparse due to the local nature of the interactions: That is to say, the number of nonzero entries in the Hamiltonian matrix is far smaller than the number of vanishing entries. For example, a geometrically d -dimensional lattice of L^d spin- $\frac{1}{2}$ has a total Hilbert-space dimension of 2^{L^d} and, thus, a $2^{L^d} \times 2^{L^d}$ Hamiltonian matrix. This sparseness is relevant both for our construction of the time evolution operator (discussed in this section) as well as for the construction of the restricted Hilbert space $\mathcal{H}_{\text{eff}}(t)$ (discussed in the following section). We begin by demonstrating the sparse nature of some common models.

If we choose the basis to be the tensor product of the local σ_z basis, then the number of nonzero elements of a purely local Hamiltonian $H_0 = \sum_k \epsilon_k \sigma_z^{(k)}$ is of course 2^{L^d} . In the same basis, a nearest-neighbor (NN) interac-

tion Hamiltonian of the type

$$\sum_{\substack{j,k \\ j,k \in \text{NN}}} v_{j,k} \sigma_x^{(j)} \sigma_x^{(k)}$$

adds $4d(L-1)L^{d-1}2^{L^d-2}$ matrix elements. Thus, a Hamiltonian that combines these two typical interaction terms will have a density of

$$\frac{2^{L^d} + 4d(L-1)L^{d-1}2^{L^d-2}}{2^{2L^d}} = \frac{1 + d(L-1)L^{d-1}}{2^{L^d}},$$

indicating that its density decreases rapidly as either of L or d increases.

As a second example, the single-particle TB Hamiltonian (2) has a total Hilbert space dimension of L , with L diagonal and $2(L-1)$ off-diagonal elements, leading to a matrix density of $(3L-2)/L^2$. Compared to the (many-body) spin Hamiltonian, this model is relatively less sparse because only the single-particle subspace is maintained, but the density still decreases according to a power law for large L .

Finally, consider the density of the single-exciton Holstein model Hamiltonian as given in (3), but with a fixed truncated maximum local phonon number d_{pho} and a chain length L . The total Hilbert space dimension of such a model is $\dim \mathcal{H} = L(d_{\text{pho}})^L$, and therefore a dense representation of the corresponding Hamiltonian will contain a total of $L^2(d_{\text{pho}})^{2L}$ matrix elements. Even for a small example system of $L=9$ and $d_{\text{pho}}=5$ and assuming that each entry is saved as a 64-bit floating point number, such a matrix would already require over 2248 TiB of memory to represent, clearly out of reach of current computing power. However, once again, most matrix elements in the Hamiltonian are zero, as the density of the Holstein Hamiltonian H_{H} with a fixed local phonon cutoff can be found to be

$$\frac{1}{L^2 d_{\text{pho}}^L} \left[(5L-2) - \frac{2L}{d_{\text{pho}}} \right]. \quad (4)$$

Here, the density once again decreases exponentially with chain length due to the quasi-many-body nature of the phonons. If we plug in the same $L=9$ and $d_{\text{pho}}=5$, we get approximately 587 MiB for 64-bit floats, less than $\frac{1}{4\,000\,000}$ of the dense matrix.

The use of sparse matrices requires saving some additional information about the position of a certain value in the matrix, which entails some memory overhead, yet for all but the smallest matrices, the relative contribution of this overhead is so negligibly small as to make the sparse matrix representation worthwhile nonetheless. For example, in one of the simplest, albeit also one of the most inefficient sparse matrix formats, the ‘‘coordinate’’ or COO format, the coordinates of each non-zero matrix element are saved explicitly. This induces a constant scaling increase in the memory requirement of the sparse matrix, independent of its specific structure. In

practice, the COO format is used to construct the sparse matrices in *paces*, but the matrices are then immediately converted to the more memory-efficient CSR (compressed sparse row) format, which also allows for more efficient sparse matrix-vector operations (SpMV) than COO⁵⁰.

1. Evaluating the action of the dense propagator matrix

After having established that sparse matrices are very efficient representations of many common many-body Hamiltonians, we are faced with one more crucial issue: The time evolution operator $U(\delta t) = e^{-iH\delta t/\hbar}$ is, in general, not sparse. Intuitively, one may easily see this by considering the following: Though the Hamiltonian matrix may be sparse due to the local nature of the interactions, $U(\delta t)$ contains all powers of H and therefore contains many combination of all local interactions, such that it generally lacks this property of locality. In other words, if there is any non-zero transition probability S_{jk} between two states for some time δt (which is likely the case if the two states are not separated for some symmetry reasons), then the time evolution operator matrix element $U_{jk}(\delta t)$ between those two states is also non-zero. Though this transition probability may be infinitesimally small for almost all pairs (j, k) , the propagator matrix will nevertheless not be representable as a sparse matrix without further approximation (unlike the Hamiltonian, which is often sparse without any approximation). Though it may seem as if all of the above analysis on sparseness is thus wasted, such is not the case.

The remedy lies in not explicitly calculating $U(\delta t)$ and then letting this operator act on the state vector, but to rather apply each individual term of the Taylor series expansion (i.e., each power of H) to the state vector individually and calculate the running sum; the algorithm that is implemented is a simplification of a scaling-and-squaring method for $e^A B$ described by Higham and Al-Mohi⁵¹. In other words, instead of calculating

$$U(\delta t) = \sum_{n=0}^N \frac{(-i\delta t H/\hbar)^n}{n!},$$

which would be a dense matrix which we could apply to $|\psi\rangle$, we instead immediately apply the action of each $\frac{-i\delta t/\hbar}{n} H$ to the vector and keep only the resulting vector. In `python/numpy` syntax, the core of the idea is:

```
def single_step_evolution(dt, input_vec, H, num_iter):
    current_vec = input_vec
    result = input_vec
    for n in range(1, num_iter+1):
        current_vec = H.dot(current_vec)
        current_vec *= -1j * dt/(hbar * n)
        result += current_vec
    return result
```

This method of calculation only requires keeping track of one additional vector apart from the input and output vector, instead of needing to save an entire potentially dense matrix. Thus, using an efficient algorithm for

SpMV operations, of which there are plenty, we can evaluate such a time evolution very memory-efficiently. This is also an advantage over the Lanczos algorithm, which, in this situation, would be far less memory-efficient, as it requires storing multiple such vectors (see appendix A).

B. Co-evolving subspaces

In section II, we alluded to the concept of “neighboring” basis states which span the adapted effective Hilbert space. We will now describe how these neighboring basis states are determined, which, as mentioned above, is very similar to the procedure underpinning the limited-functional-spaces method³⁶.

1. Motivation

As an illustrative example, consider a simple single-particle tight-binding chain (2) of infinite length. Say we have, at time $t = 0$, a particle completely localized at site $|n\rangle$, which we know will spread ballistically over time. At time $t_1 > 0$, the system has evolved to be mostly localized on over the five sites

$$\{|n-2\rangle, |n-1\rangle, |n\rangle, |n+1\rangle, |n+2\rangle\}.$$

If we were to poorly apply the Hilbert subspace arguments from section II and neglect all basis states which are currently not occupied, we could calculate the dynamics only within these five basis states, but doing so would prevent the wavepacket from further spreading ballistically, which is clearly a poor representation of the actual physics. The solution for the problem is clear in this example: We should include the next few sites in the chain so that the system can freely evolve into the neighboring states, while still neglecting the very far-away states which will not be occupied within the next timestep. However, though this concept of neighboring states is evident in a well-ordered chain, how should we determine which basis states are “neighbors” in a basis without an obvious ordering?

2. Defining neighboring basis states

Since we are interested in the time evolution, which is ultimately governed by the Hamiltonian, a reasonable answer to this question is to consider the structure that the Hamiltonian itself induces on the basis states. Let \mathfrak{B} be the orthonormal basis in which we are representing our vectors and matrices, with $\text{span } \mathfrak{B} = \mathcal{H}$ the total Hilbert space. As a linear operator, the Hamiltonian maps each

basis state $|n\rangle \in \mathfrak{B}$ onto another state

$$\begin{aligned} H|n\rangle &= \sum_{|k\rangle \in \mathfrak{B}} h_{kn} |k\rangle \\ &= \sum_{|m\rangle \in \mathcal{N}_{|n\rangle} \subset \mathfrak{B}} h_{mn} |m\rangle + \sum_{|k\rangle \in \mathfrak{B} \setminus \mathcal{N}_{|n\rangle}} 0 |k\rangle, \end{aligned}$$

where the set of basis states $\mathcal{N}_{|n\rangle}$ corresponds to the subset of all basis states in \mathcal{H} that $|n\rangle$ is mapped onto under H , or symbolically:

$$\mathcal{N}_{|n\rangle} := \{|m\rangle \in \mathfrak{B} \mid \langle m|H|n\rangle \neq 0\}.$$

This definition readily extends to a state $|\psi\rangle$ which is not a basis state, or even an arbitrary set \mathcal{M} of basis states (which may also be identified with the subspace it spans):

$$\begin{aligned} \mathcal{N}_{|\psi\rangle} &:= \{|n\rangle \in \mathfrak{B} \mid \langle n|H|\psi\rangle \neq 0\}, \\ \mathcal{N}_{\mathcal{M}} &:= \{|n\rangle \in \mathfrak{B} \mid (\exists |m\rangle \in \mathcal{M}) [\langle n|H|m\rangle \neq 0]\}. \end{aligned} \quad (5)$$

We can now use this definition to call $\mathcal{N}_{\mathcal{M}}$ the *neighboring states of \mathcal{M}* . Note that $|n\rangle$ may be contained in $\mathcal{N}_{|n\rangle}$, for example when H has a non-zero diagonal element h_{nn} —if this is the case, call $|n\rangle$ a *trivial neighbor* of \mathcal{M} . We can also easily generalize (5) to “higher-order” neighbors:

$$\mathcal{N}_{\mathcal{M}}^{(k)} := \{|n\rangle \in \mathfrak{B} \mid (\exists |m\rangle \in \mathcal{M}) [\langle n|H^k|m\rangle \neq 0]\}. \quad (6)$$

The set $\mathcal{N}_{\mathcal{M}}^{(k)}$ then denotes the set of basis states into which the set of states \mathcal{M} can evolve under k -fold application of the Hamiltonian. Furthermore, note that $\mathcal{N}_{\mathcal{M}}^{(0)} = \mathcal{M}$.

Let us illustrate this concept for first-degree neighbors, $k = 1$, using the TB model (2). Let \mathcal{M} be the set consisting of the two basis states

$$\mathcal{M} = \{|n-1\rangle, |n+1\rangle\}.$$

The TB Hamiltonian with a constant hopping parameter $J_k = J$ and zero on-site energy $\epsilon_k = 0$ maps the first state $|n-1\rangle$ onto

$$|n-1\rangle \mapsto J(|n-2\rangle + |n\rangle) \in \text{span}\{|n-2\rangle, |n\rangle\},$$

and maps the second state onto

$$|n+1\rangle \mapsto J(|n\rangle + |n+2\rangle) \in \text{span}\{|n\rangle, |n+2\rangle\}.$$

Therefore, in this case the neighbor set is

$$\mathcal{N}_{\mathcal{M}} = \{|n-2\rangle, |n\rangle, |n+2\rangle\},$$

which is precisely what one would intuitively expect when speaking of the neighboring lattice sites of $\{|n-1\rangle, |n+1\rangle\}$. If the on-site energy is non-zero, $\epsilon_{n\pm 1} \neq 0$, then $|n-1\rangle$ is also mapped to itself and similarly for $|n+1\rangle$, such that the neighbor set becomes

$$\mathcal{N}_{\mathcal{M}} = \{|n-2\rangle, |n-1\rangle, |n\rangle, |n+1\rangle, |n+2\rangle\},$$

where we can see that $\mathcal{M} \cap \mathcal{N}_{\mathcal{M}} = \mathcal{M}$, i.e., $\mathcal{N}_{\mathcal{M}}$ now contains trivial neighbors.

The effective Hilbert space that is used to evolve $|\psi\rangle$ from time t to $t + \delta t$ is constructed as

$$\mathcal{H}_{\text{eff}}(t) = \text{span} \left\{ \bigcup_{k=0}^m \mathcal{N}_{|\psi(t)\rangle}^{(k)} \right\}. \quad (7)$$

In practice, the maximum neighbor degree m is usually on the order of 20 for the initial generation at $t = 0$, but a small number such as 2 is chosen when dynamically adapting at $t > 0$. The LFS method, by contrast, only performs the initial adaptation at $t = 0$ and then evolves within the fixed space.

On a theoretical level, this procedure of “neighbor-finding” induces a (weighted and undirected) graph on the basis states of the Hilbert space. This Hamiltonian-induced graph structure is precisely what determines how closely or distantly different basis states are related for our purposes. This line of thought has previously been used in the study of continuous-time quantum walks⁵² and thermalization and ergodicity in quantum systems^{53–55}.

An important and useful feature of this approach should be noted: If the Hamiltonian H under consideration induces a symmetry S of the system ($[H, S] = 0$) and the state ψ that is being evolved lies fully within one symmetry sector ($S|\psi\rangle = \lambda|\psi\rangle$ where λ is some number), then the neighbor-states approach described here will automatically respect that symmetry and never include basis states belonging to a different symmetry sector. For example, the effective Hilbert spaces constructed for a state with a definite particle number that is evolving under a particle-number-conserving Hamiltonian will automatically be restricted to the appropriate particle-number subspace. This behavior can potentially greatly increase numerical efficiency without any further user input. Such behavior may also be realized, for example, in MPS methods, but requires additional effort to be invested in symmetrization^{56–58}.

Furthermore, we point out that the time-evolution operator inside \mathcal{H}_{eff} is typically expanded to a much higher degree than the maximal neighbor degree with which \mathcal{H}_{eff} is constructed: This allows for near-unitary and virtually exact time evolution *within the restricted subspace*. Since the evaluation of the time evolution operator as described in section III A is very efficient in both computational time and memory, there is little reason not to use as high an order as possible and calculate the single-step time evolution with as much accuracy as possible. Furthermore, an m -th-order neighboring subspace guarantees that all neighboring states up to order m are *included*, but it does *not necessarily exclude* all neighbors of order $m + 1$ and higher, as a typical delocalized state will already contain many of its own neighboring basis states.

3. Comparison with Krylov subspaces

Superficially, the concept of $\text{span} \left\{ \bigcup_{k=0}^{m-1} \mathcal{N}_{\mathcal{M}}^{(k)} \right\}$ may seem similar to the Krylov subspace K^m , defined as^{59,60}

$$K^m(H, v) = \text{span} \{ v, Hv, H^2v, \dots, H^{m-1}v \},$$

In fact, the two are, however, quite different: This can be easily seen by considering that the Krylov subspace K^m is (at most) an m -dimensional vector space, whereas the dimension of m -degree neighbor sets is typically far larger than m . Vectors within, e.g., $K^2(H, v)$ may only be composed of a superposition of v itself and Hv ; on the other hand, the dimension of $\text{span} \left\{ \mathcal{N}_v^{(k)} \right\}$ is typically much larger than k , and depends on both the basis in which the system is expressed as well as the nature of both H and v . For example, returning to the TB example set $\mathcal{M} = \{|n-1\rangle, |n+1\rangle\}$ —a very small set to begin with—we find that (with $\epsilon = 0$)

$$\left| \mathcal{N}_{\mathcal{M}}^{(0)} \right| = |\mathcal{M}| = 2, \quad \left| \mathcal{N}_{\mathcal{M}}^{(1)} \right| = 3, \quad \left| \mathcal{N}_{\mathcal{M}}^{(2)} \right| = 4,$$

leading to

$$\mathcal{N}_{\mathcal{M}}^{(0)} \cup \mathcal{N}_{\mathcal{M}}^{(1)} \cup \mathcal{N}_{\mathcal{M}}^{(2)} = \{|n-3\rangle, |n-2\rangle, \dots, |n+3\rangle\},$$

which spans a seven-dimensional vector space—note that the subadditive nature is due to $\mathcal{N}_{\mathcal{M}}^{(0)} \subsetneq \mathcal{N}_{\mathcal{M}}^{(2)}$. On the other hand, if we were to form an arbitrary vector out of the constituent vectors of \mathcal{M} , e.g.,

$$|\psi\rangle = \frac{1}{\sqrt{2}} (|n-1\rangle + |n+1\rangle) \in \text{span } \mathcal{M},$$

then the corresponding Krylov subspace K^3 would always be of dimension 3 (regardless of the precise coefficients) and consist of

$$\begin{aligned} K^3(H_{\text{TB}}, |\psi\rangle) = \text{span} \{ & (|n-1\rangle + |n+1\rangle), \\ & (|n-2\rangle + 2|n\rangle + |n+2\rangle), \\ & (|n-3\rangle + 3|n-1\rangle + 3|n+1\rangle + |n+3\rangle) \}, \end{aligned}$$

clearly a quite different result from the neighboring-states constructions: For example, the state $|n\rangle$ is not contained in this subspace.

It is, in principle, possible to construct $\bigcup_{k=0}^{m-1} \mathcal{N}_{|\psi\rangle}^{(k)}$ from K^m by identifying the basis states $|n\rangle \in \mathfrak{B}$ contained in the Krylov space:

$$\bigcup_{k=0}^{m-1} \mathcal{N}_{|\psi\rangle}^{(k)} = \{ |n\rangle \in \mathfrak{B} \mid (\exists |\chi\rangle \in K^m) [\langle n|\chi\rangle \neq 0] \},$$

however, this connection is arguably not of particular value.

4. Application to time evolution & post-adaptation detruncation

paces uses (7) to construct the effective Hilbert space based on a preset maximum neighbor degree m . The accuracy of the results is of course improved with increasing m , but the memory required to save the vectors and matrices associated with the effective Hilbert space also increases, which means that we need to truncate the state vector more harshly if we wish to include higher-degree neighbors. Therefore, it is necessary to find a compromise between truncation and the neighbor degree.

However, there is a subtle but important trick that can be used in the interplay between truncation and adaptation: After the new effective Hilbert space has been determined, one can “rescue” any possible values that had originally been marked for truncation but whose basis states were reinstated by the adaptation. More specifically: Say we want to truncate the state vector $|\psi(t)\rangle$ to the M states that make up some set of basis states \mathcal{M} . This set of states \mathcal{M} is then fed into the adaptation algorithm which will produce the adapted effective Hilbert space $\mathcal{H}_{\text{eff}}(t)$ as given by (7). Now, instead of actually keeping only the M most important expansion coefficients of the vector, i.e., instead of projecting $|\psi(t)\rangle$ to span \mathcal{M} , we instead project $|\psi(t)\rangle$ to the larger Hilbert space $\mathcal{H}_{\text{eff}}(t) \supset \text{span } \mathcal{M}$, thereby (typically) truncating to a lesser extent than expected and keeping more than M expansion coefficients. In extreme cases, it is even possible that this “post-adaptation detruncation” results in no truncation at all, if $\mathcal{H}_{\text{eff}}(t - \delta t)$ is entirely contained within $\mathcal{H}_{\text{eff}}(t)$.

As a practical example, consider the simulations shown in Fig. 2: In this calculation, the nominal truncation cut-off number was set to $M = 13 \times 10^6$, but we see that the actual number of non-zero coefficients was approximately $\dim \mathcal{H}_{\text{eff}} = 7.5 \times 10^7$, which is almost an order of magnitude larger due to the “detruncation” procedure we just described.

5. Generating the effective Hamiltonian from the effective Hilbert space

When constructing a new effective Hilbert space, it is straightforward to construct the effective Hamiltonian within this effective Hilbert space: Since we have already generated the set of basis states $\mathcal{N}_{\mathcal{M}}^{(k)}$ by applying the Hamiltonian k times, we can simply retain those Hamiltonian matrix elements and combine them with their hermitian conjugates, which by construction also automatically must add up to *every* Hamiltonian matrix element within the effective subspace. However, we need to take care to avoid creating duplicate entries of matrix elements, which can occur, e.g., either due to the intersection of two neighbor sets being non-empty ($\mathcal{N}_{\mathcal{M}}^{(k)} \cap \mathcal{N}_{\mathcal{M}}^{(l)} \neq \emptyset$), or due to the existence of non-trivial neighbors within \mathcal{M} .

As an example for the latter, consider a set $\mathcal{S} = \{|n-1\rangle, |n\rangle\}$ under the TB Hamiltonian with $\epsilon = 0$. When creating the first set of Hamiltonian matrix elements while generating $\mathcal{M}_{\mathcal{S}}^{(1)}$, the basis state $|n\rangle$ leads to the creation of the matrix elements

$$|n\rangle \implies \{H_{n-1,n}, H_{n+1,n}\} + \text{h.c.},$$

whereas the other basis state leads to

$$|n-1\rangle \implies \{H_{n-2,n-1}, H_{n,n-1}\} + \text{h.c.}$$

Naïvely combining both of these sets of matrix elements will lead to the duplicates $H_{n-1,n}$ and $H_{n,n-1}$ because the two states $|n\rangle$ and $|n-1\rangle$ are neighboring basis states and must, by definition, map into each other. We must ensure that no such duplicates are entered into the sparse matrix, as doing so would double the value of that matrix element and thus considerably distort the Hamiltonian.

C. How to weight states for truncation

We have discussed the merits of sparse matrix representations and how to compute each individual $U(\delta t)$ using sparse matrices in section III A, as well as how to construct a reasonable adapted effective Hilbert space around a given truncated state vector in sec. III B. The last large puzzle piece that remains to be discussed is how to actually perform the truncation of a state vector after its time evolution.

The simplest approach is to simply sort the expansion coefficients by their current weight $w_0^{(n)} := |\langle n|\psi(t)\rangle|^2$ and then truncate to the M coefficients with the highest weight. Though this approach is certainly reasonable, it is not necessarily optimal: The basis states that exhibit the highest weight in the wavefunction at time t are not necessarily those that bear the greatest importance for the future of the time evolution. One might, therefore, consider estimating the future “importance” of the basis state $|n\rangle$ by weighting it not by $|\langle n|\psi(t)\rangle|^2$, but rather by some method that assigns additional weight to highly connected states that may be explored in the next timestep, for example:

$$|\langle n|\psi(t+\tau)\rangle|^2 \approx \left| \langle n| \left(1 - \frac{i\tau}{\hbar} H \right) |\psi(t)\rangle \right|^2 =: w_\tau^{(n)}.$$

The future-weighting parameter τ can be varied independently of the timestep δt , and setting $\tau = 0$ results in the simple current-time weight $w_0^{(n)}$. However, in practice, said more general weighting mechanism performs best for $\tau = 0$ —i.e., the naive approach appears to be superior to any “forward-looking” weighting. Future analyses may uncover better weighting methods than the naive one, which would allow faster convergence to be achieved.

We point out a subtlety that must be taken into account when performing the truncation, regardless of

which weighting method is employed: Especially in symmetric systems, the weighting method may result in degenerate weights, and if there is a recurring but incidental order to the states prior to truncation, the truncation may introduce unwanted biases. For example, let the truncation happen after the q highest-weighted basis states, and let the q -th basis state be $|n_1, \dots, n_L\rangle$. If the weight of the basis state $|n_1, \dots, n_L + 1\rangle$ is identical to that of $|n_1, \dots, n_L\rangle$ and the states are always sorted lexicographically prior to the truncation, then there will be an unwanted bias towards the state $|n_1, \dots, n_L\rangle$. One way to circumvent this issue and avoid such a bias is to (pseudo-)randomize the order of degenerate-weight states around the cutoff point.

D. Summary and notes on parallel implementation

We can now give a more precise description of the procedure that was outlined in section II: To evolve a state $|\psi(t)\rangle$ with a sparse representation in the basis \mathfrak{B} forward by one timestep:

1. First construct the effective Hilbert space $\mathcal{H}_{\text{eff}}(t)$ as described in (7). Formally, we can define P_m to be the projector onto $\mathcal{H}_{\text{eff}}(t)$, where m is the maximal neighbor degree, although we do not construct such a projection operator numerically.
2. Then evolve $|\psi(t)\rangle$ within this Hilbert space. This can be formally written as $\tilde{U}(\delta t) = \exp(-iP_m H P_m \delta t / \hbar)$.
3. Finally, if necessary, truncate the resulting state using the weighting method described above. This truncation can also be formally described as a projector Q , though no such projection operator is actually constructed.

Thus, the action of a full step of the algorithm can be formally described as the mapping

$$|\psi(t)\rangle \mapsto Q \exp(-iP_m H P_m \delta t / \hbar) |\psi(t)\rangle,$$

where the essence of the method lies, formally speaking, in the construction of Q and P_m . We will use the same terminology to discuss error scaling behavior in section V.

One of the main advantages of the present method is that all of the aforementioned components lend themselves very well to parallel execution on GPUs, enabling substantial speedups compared to sequential execution of the method. More precisely, the computation of $\exp(-iP_m H P_m \delta t / \hbar)$ from the restricted Hamiltonian $P_m H P_m$ is fully parallelized, as it is performed via the repeated application of the Hamiltonian to the state, which can be done using existing highly efficient SpMV algorithms. Applying the truncation Q is computationally trivial, but determining the set to be truncated, in the

current implementation, relies on a combination of sorting and searching. The latter is implemented concurrently but is relatively diverging and therefore not entirely optimal. Finally, determining $\mathcal{H}_{\text{eff}}(t)$ is once again simply a repeated application of SpMV operations and, therefore, highly parallelized, but transferring the state $|\psi(t)\rangle$ from one effective Hilbert space to the next relies on matching up different indices, which is a rather highly divergent problem and is currently the efficiency weak point of the method. Overall though, the method profits enormously from mostly well-parallelizable subproblems and performs well on GPUs, the largest limiting factor in many practical situations being the limited RAM that is available on GPUs and which is required for less harsh truncation steps or high-order neighbor states.

MPS methods, as a counterexample, have their strength in the local decomposition (and efficient truncation) of an exponentially large wavefunction, which allows for simpler local manipulations on the individual matrices. While this decomposition has its benefits, it also brings with it drawbacks such as the need for system sweeps, which are necessarily sequential and make for poor parallelization: There have been recent efforts towards efficient GPU implementations of MPS methods (e.g., 61–64), which are often, however, limited by the SVD or QR decomposition, which lends itself poorly to parallelization. On the other hand, the present algorithm features no such local decompositions at all, allowing the system to be tackled in its entirety all at once and enabling easier parallelization. This, of course, is a double-edged sword: In pursuit of parallelization, we are required to manipulate the entire dataset simultaneously, i.e., it becomes necessary to store the entire state vector, matrices etc. in readily accessible RAM. As GPU RAM size is currently often still an order of magnitude or more below what is available for CPUs, this is the main practical computational limitation of the method, though “unified memory” can alleviate this problem at the expense of becoming memory-bandwidth-limited. We note that the parallelized and sparse nature of our method makes useful computations of time-complexity highly involved, in part due to non-negligible I/O and memory access times relative to actual computational time⁶⁵.

IV. INFORMATION CONTENT COMPARISON WITH MPS

As MPS methods are some of the most widespread numerically exact techniques in condensed-matter physics, allowing for often highly efficient tensor-based representations of quantum states, one may wonder how the “information density” of a tensor-based representation compares to the present sparse- or truncated-vector-based method. We shall now compare the memory required to store a given state in MPS or the *paces* method using a few examples states.

It is well-known that MPS work well for weakly-

entangled states in one-dimensional lattice systems, as the truncation and representation are intertwined with the geometrical structure of the lattice. On the other hand, though the present method is completely agnostic of the geometry of the underlying system it depends strongly on how well the chosen basis represents a given state. Both of these characteristics can work for or against either method, which we shall elucidate using some simple example states. All of the following example states shall be states in a Hilbert space $\mathcal{H} = \mathcal{H}_{\text{qudit}}^{\otimes L}$ describing a length- L chain of d -dimensional qubits.

A. Example 1

An almost trivial example of how MPS compression can beat wavefunction truncation is the following state

$$|\psi_{\text{delocal}}\rangle = \frac{1}{d^{L/2}} \sum_{\sigma_1, \dots, \sigma_L} |\sigma_1, \dots, \sigma_L\rangle,$$

which could be considered “completely delocalized” on the given basis, is exactly representable as an MPS with bond dimension $\chi_{\text{max}} = 1$ using

$$A_{\sigma_i} = \left(\frac{1}{\sqrt{d}} \right)$$

for every lattice site i and basis state σ . This is, of course, due to the fact that this state is completely unentangled; it can be rewritten as a product state

$$|\psi_{\text{delocal}}\rangle = \left(\sum_{\sigma_1} \frac{1}{\sqrt{d}} |\sigma_1\rangle \right) \otimes \dots \otimes \left(\sum_{\sigma_L} \frac{1}{\sqrt{d}} |\sigma_L\rangle \right),$$

which is virtually the best case scenario for MPS. The present coefficient truncation method, on the contrary, would struggle as much as possible with such a state, as the smallest effective Hilbert space that would capture this state vector exactly is the entire Hilbert space itself, and due to the complete degeneracy of the expansion coefficients, every choice for a truncation would be equally bad. However, this deficiency is completely basis-dependent, as we could in principle unitarily rotate the single-site basis such that

$$|0'\rangle := \sum_{\sigma=0}^{d-1} \frac{1}{\sqrt{d}} |\sigma\rangle$$

such that the same state, in a different basis, reads

$$|\psi_{\text{delocal}}\rangle = |0'\rangle^{\otimes L},$$

which is exactly representable by a single expansion coefficient.

B. Example 2

Despite the discouraging first example, naturally, there are cases in which the MPS representation is not optimal.

As the first example showcased the strength of MPS for unentangled states, it is natural to consider the opposite case, a maximally entangled state. In the same d^L -dimensional Hilbert space, consider now the generalized Bell state

$$|\psi_{\text{Bell}}\rangle = \frac{1}{\sqrt{d}} \sum_{k=0}^{d-1} |kk \dots kk\rangle.$$

Along any bipartition of the lattice, this state has entanglement $\log_2 d$, and therefore its MPS representation requires a bond dimension⁶⁶ of $\chi_{\text{max}} = d$. Thus, even for $L = 3$, the central tensor alone requires storing a total of $d \times d \times d$ matrix elements. The number of non-zero expansion coefficients, on the other hand, is simply d , resulting in a drastically lower amount of information that needs to be stored in the vector-truncation method.

C. Example 3

The first two examples covered the more or less obvious fact that MPS are well suited as exact representations of weakly entangled states and poorly suited to represent highly entangled states. One can, however, construct a more subtle and unrelated example, which highlights the fact that MPS representations struggle with large local dimensions d (which becomes particularly relevant for, e.g., harmonic oscillators). Consider now, in the same general Hilbert space as before, the very simple state

$$|\psi_0\rangle = |00 \dots 00\rangle.$$

This is a single basis state and therefore completely unentangled, therefore it requires a bond dimension of only $\chi_{\text{max}} = 1$, just as in example 1. However, if L or d is large, then an MPS representation will still be rather inefficient, as it still needs to store L third-order tensors of dimension $d \times 1 \times 1$ each, even though there is only a single non-zero expansion coefficient. The deciding factor here is that if we choose a Hilbert space that is too large in either way (locally, d , or globally, L), then over the entire course of the simulation we will always pay the price of having to store unnecessary zeros.

D. Example 4

We can combine the problems demonstrated in examples 2 and 3 by considering the generalized NOON state:

$$|\psi_{\text{NOON}}\rangle = \frac{1}{\sqrt{2}} (|00 \dots 01\rangle + |10 \dots 00\rangle).$$

Equivalently, this can be seen as a standard binary Bell state which has been separated over a large distance. The $\log_2 2$ entanglement requires a bond dimension of $\chi_{\text{max}} = 2$ on every site: In other words, in order to pipe this rather weak entanglement through the entire

TABLE I. The number of values (matrix elements or vector coefficients) that need to be stored to represent each state exactly using either matrix-product states or the truncated/sparse vector representation. Note that we are discounting the index information that also needs to be stored when using the vector truncation method, which results in a roughly constant scaling of said results by a factor of ~ 3 .

state	MPS	sparse-vector rep.
$ \psi_{\text{delocal}}\rangle$	dL	d^L
$ \psi_{\text{Bell}}\rangle$	$2d^2 + (L - 2)d^3$	d
$ \psi_0\rangle$	dL	1
$ \psi_{\text{NOON}}\rangle$	$4d(L - 1)$	2

system, it is necessary to waste memory at every lattice site connecting the two; additionally, it is necessary to store empty information on the unoccupied basis states $|2\rangle, |3\rangle, \dots$ at every site. This is where the state vector truncation method shines most due to its system-agnostic nature. It knows of neither the fact that the two basis states represent an entangled state, nor of the fact that this entanglement is long-ranged, and requires saving only the two non-zero expansion coefficients.

This example may seem contrived and unphysical, as one may argue that long-range correlations are rather rare and would realistically be subject to considerable decoherence in natural systems. However, situations such as this may indeed arise in practice if the system is not geometrically one-dimensional and it was necessary to force a linear ordering upon a system; for example, two neighboring sites in 3D are not necessarily neighboring when ordered in 1D, leading to seemingly long-ranged entanglement.

E. Summary

A quantitative comparison of the above examples is given in Table I. We have determined that, as expected, MPS works very well for states with low or locally confined entanglement, whereas the method of vector expansion coefficient truncation naturally excels in situations in which the given basis leads to a sparse representation of the state vector. Vector truncation is agnostic of entanglement and, as such, depends more strongly on the amount of coherence in the given basis. MPS, on the other hand, due to its indifferent handling of zero-weight basis states, is less efficient when the entire chosen Hilbert space is large, even if outlying basis states do not actually occur in a given state.

Two important consequences of this are: First, since entanglement is invariant under local unitary transformations⁶⁷, this limitation of MPS cannot be remedied (but also not exacerbated) by a local change of basis, whereas the vector truncation method can be ameliorated or deteriorated by a good or poor choice of basis. However,

it should be noted that both methods can be affected by *non-local* basis transformations: If a non-local basis transformation decreases long-range entanglement, MPS methods can be expected to perform better, whereas a non-local basis transformation that concentrates the wavefunction on a smaller number of basis states will benefit *paces*. Second, standard MPS representations encounter fundamental limitations when dealing with large or infinite local dimensions, since in such cases it becomes necessary to drag along many basis states (physical indices) which may be completely unnecessary at the current time, while the state vector truncation method on the other hand is suitable for applications with a very large number of unoccupied basis states surrounding the current state vector. The issues encountered by MPS in these examples could be partially alleviated by employing sparse tensors or by reordering the system indices, though the latter likely requires manual fine-tuning and prior knowledge of the dynamics. Furthermore, efforts such as LBO mentioned in section I have been developed to combat large local physical dimensions, but such methods also require investing additional computational resources to solve the problem.

In summary, the suitability of the given basis can make or break the ability of the truncated-vector method to represent a given state and subsequently the feasibility of *paces*. However, finding the optimal basis for the present method requires finding a delicate balance between the complexity of the dynamics and the sparseness of the Hamiltonian matrix. For example, the Lang-Firsov or polaron transformation^{68,69} may be beneficial to solving the Holstein Hamiltonian in that it locally transforms the problem such that off-diagonal elements of the Hamiltonian become smaller, but it also makes the Hamiltonian much less sparse due to quasi-non-local couplings in the new basis.

Though the examples given above may be illustrative, they have so far only considered exact representations of a given state: Further systematic investigation and comparison of the loss of information when a state is *compressed* in either of the two schemes would be interesting and relevant for future developments.

V. PERFORMANCE & ERROR ANALYSIS

In this section, we shall first investigate the origin and behavior of the errors induced by this method—that is to say, the deviations between the true time-evolved state and the time-evolved state as computed using *paces*—and then show actual numerical behavior, both relative to the method itself and compared to existing MPS calculations.

A. General error analysis

We first distinguish between the different possible sources of deviations from the true time evolution and de-

termine their relative importance to the overall accuracy. We re-use the terminology of P_m and Q that was established in section III D here. The three principal sources of differences between the exact time evolution and the time evolution by the present method are:

1. the truncation of the time evolution operator $\exp(-iP_m H P_m \delta t/\hbar)$ after a finite number of terms in its series expansion,
2. the truncation of the state vector due to the projection Q , and
3. artifacts due to the restriction into an effective Hilbert space with only m -th-order neighbors, as given by the projection P_m .

The error due to the truncation of the series expansion of the time-evolution operator is essentially negligible in practice, as the series is only terminated once a set convergence criterion has been reached due to its relatively “cheap” numerical nature that does not necessitate earlier truncation. This conclusion is supported by the data presented in section V B; we refer the reader to the more detailed analysis provided in references 51 and 70 for detailed error analysis and consider the error to be negligible compared to the other errors encountered in our method.

The error induced by the truncation Q , measured in terms of the wavefunction norm, is simply $\|\psi - Q|\psi\rangle\|$. The size of this error depends on the distribution of the expansion coefficients $|\langle n|\psi\rangle|^2$. The exact nature of this distribution must depend on the Hamiltonian, the initial state and the basis that is chosen: Finding a general law predicting (at least asymptotically) the distribution of the expansion coefficients would, arguably, answer a rather profound question on fundamental quantum mechanics, but at the same time, taming this distribution lies at the heart of *paces*, so we will consider two different educated guesses. For example, if we assume that the expansion coefficients in the basis \mathfrak{B} decay exponentially, $|\langle n|\psi\rangle|^2 \propto \alpha^n$ for some $\alpha \in (0, 1)$, then if \mathfrak{B} is countably infinite, the truncation error due to projecting onto the q highest-weight basis states is given by

$$\|\psi - Q|\psi\rangle\| = \sqrt{\sum_{k=q}^{\infty} |c_k|^2} = \alpha^{q/2},$$

that is, if the coefficients decay exponentially, then the error induced by each truncation also decays exponentially as a function of the number of basis states q that the state is projected onto. Naturally, this means that if the decay of the coefficients can be upper-bounded by some exponential function, then the error features the same kind of exponential upper bound. Because of this, an exponential distribution is a rather optimistic viewpoint on the possible distribution of coefficients. Potential hand-waving justifications for an exponential distribution could be based on Lieb–Robinson-type arguments,

Anderson localization, or simply on the idea that an initially “localized” (in \mathcal{H}) state may spread exponentially under a time-evolution operator $e^{-iH\delta t/\hbar}$, but none of these arguments are even close to rigorous.

On the other hand, a much more pessimistic but potentially also realistic distribution could be a power law: $|\langle \psi|n\rangle|^2 \propto 1/n^s$ with $s \geq 1$ —where $s = 1$ corresponds to Zipf’s law, which is, however, not normalizable if the Hilbert space is infinite-dimensional. The truncation error in the case of a power law can be computed to be

$$\varepsilon(Q) = \|\psi - Q|\psi\rangle\| = \sqrt{\frac{1}{\zeta(s)} \sum_{k=q+1}^{\infty} \frac{1}{n^s}},$$

where $\zeta(s)$ is the Riemann zeta function which normalizes the coefficients. We can bound this error by the standard Maclaurin–Cauchy integral technique to obtain:

$$\frac{1}{\sqrt{\zeta(s)(s-1)(q+1)^{s-1}}} \leq \varepsilon(Q) \leq \sqrt{\frac{\frac{1}{q+1} + \frac{1}{s-1}}{\zeta(s)(q+1)^{s-1}}}.$$

This means that, asymptotically, the error induced by the truncation Q under a power law is

$$\varepsilon(Q) = \mathcal{O}\left(q^{-\frac{s-1}{2}}\right). \quad (8)$$

It should be noted that the parameter q contained in Q is not exactly equal to the nominal truncation parameter that is set by the user due to the detruncation procedure described in section III B 4. The true q is typically significantly larger than the nominal truncation parameter (see, e.g., Fig. 5d).

Finally, we turn to the error induced by restricting the evolution of the state to the restricted subspace $\mathcal{H}_{\text{eff}}(t)$ up to order m as given in (7). This error can be quantified in the following way:

$$\varepsilon(P_m) := \left\| U(\delta t) |\psi(t)\rangle - \tilde{U}(\delta t) |\psi(t)\rangle \right\|$$

where $\tilde{U}(\delta t)$ is the time-evolution operator restricted to the m -th-order subspace $\mathcal{H}_{\text{eff}}(t)$ and P_m is the projector onto said subspace:

$$\tilde{U}(\delta t) |\psi(t)\rangle = \sum_{l=0}^{\infty} \frac{(-i\delta t/\hbar)^l (P_m H P_m)^l}{l!} |\psi(t)\rangle.$$

By the construction of $\mathcal{H}_{\text{eff}}(t)$, the projection acts trivially on all terms with indices $l \leq m$, such that

$$(P_m H P_m)^l |\psi(t)\rangle = H^l |\psi(t)\rangle \quad \text{for } l \leq m,$$

and only for terms with $l > m$ may $(P_m H P_m)^l |\psi(t)\rangle$ and $H^l |\psi(t)\rangle$ differ. Letting $Q_m := \mathbb{1} - P_m$, we can write

$$\begin{aligned} & (U(\delta t) - \tilde{U}(\delta t)) |\psi(t)\rangle \\ &= - \sum_{l=m+1}^{\infty} \sum_{\bar{\sigma}} \frac{(-i\delta t)^l A_{l-m}^{\bar{\sigma}} H^m}{l! \hbar^l} |\psi(t)\rangle, \end{aligned}$$

where

$$A_{l-m}^{\vec{\sigma}} := (-Q_m)^{\sigma_1} H (-Q_m)^{\sigma_2} H \cdots (-Q_m)^{\sigma_{l-m}} H$$

and the sum over $\vec{\sigma}$ is over all strings $(\sigma_1, \sigma_2, \dots, \sigma_{l-m})$ of length $l-m$ with binary entries $\sigma_i \in \{0, 1\}$ where at least one of the $\sigma_i \neq 0$. We will now determine an upper bound for the restriction error $\varepsilon(P_m)$: Define

$$u_l = \max_{\vec{\sigma}} \|A_{l-m}^{\vec{\sigma}} H^m |\psi(t)\rangle\|.$$

If there exists some $\alpha \in \mathbb{R}^+$ such that $u_l \leq \alpha^l$ for any l , then the error is bounded by

$$\varepsilon(P_m) \leq \sum_{l=m+1}^{\infty} \frac{2^{l-m} - 1}{l!} \left(\frac{\alpha \delta t}{\hbar}\right)^l,$$

or in the limit of small δt :

$$\varepsilon(P_m) \leq \frac{1}{(m+1)!} \left(\frac{\alpha \delta t}{\hbar}\right)^{m+1}. \quad (9)$$

The difficulty here will lie in determining α . One may simplify the expression for α by further loosening the bound, since

$$u_l \leq \|H^l |\psi(t)\rangle\| \leq (\|H\|_{\text{op}})^l$$

and therefore $\alpha \leq \|H\|_{\text{op}}$, but then the bound is hardly useful in practical terms, as it has lost all information about the underlying structure of the restricted Hilbert spaces.

An important question to consider is: How can one distinguish between these three sources of errors in a calculation? The first two errors are relatively simple to detect: An improperly truncated time-evolution operator will most likely not be unitary, such that one can compare the norm and potentially other conserved quantities such as the total energy before and after the application of the time-evolution operator to determine whether such an error is present. Similarly, the truncation error due to Q has an immediate effect on the norm of the wavefunction and its effect is largely quantifiable by measuring the discarded weight. The error due to the restriction to the effective Hilbert space via P_m , on the other hand, is rather devious, as it will not affect the norm of the wavefunction. An overly restrictive projection P_m will essentially give rise to finite-size effects such as reflections at “boundaries” in an abstract sense, which do not render the state unphysical in any sense, but will instead effect good convergence to a wrong result. The main remedies here are to either increase the maximal neighbor degree m (greatly increasing memory requirements) or to decrease the timestep δt (increasing time requirements), both of which will reduce the error induced by P_m , as shown in (9).

B. Benchmarking with a Holstein system

We use the MPS calculations of Holstein dynamics given by Kloss et al. in 71 as a reference, whose main observable of interest was the electronic root-mean-square deviation (RMSD), defined as the standard deviation of the excitonic⁷² position distribution function. The latter is

$$P(X_{\text{exc.}} = x_n) = \left\langle (b_{x_n}^{\text{exc.}})^\dagger b_{x_n}^{\text{exc.}} \right\rangle = \langle \psi | x_n \rangle \langle x_n | \psi \rangle,$$

thus, the RMSD is defined as

$$\text{RMSD} := \sqrt{\sum_{x_n=0}^{L-1} [x_n P(X_{\text{exc.}} = x_n) - \bar{X}_{\text{exc.}}]^2}, \quad (10)$$

with $\bar{X}_{\text{exc.}}$ being the average exciton position

$$\bar{X}_{\text{exc.}} = \sum_{x_n=0}^{L-1} x_n P(X_{\text{exc.}} = x_n) = \sum_{x_n=0}^{L-1} \langle \psi | x_n \rangle x_n \langle x_n | \psi \rangle.$$

The RMSD values obtained by *paces* are compared to those computed by Kloss et al. in Fig. 4.

Furthermore, we shall discuss some measurable quantities that convey information about the quality of the results without reference to external calculations. Chief among these are the *norm* of the wavefunction and the *total average energy* of the system, both of which should be conserved over the course of an exact calculation. Changes in the norm can be indicative of wavefunction truncation or of an ill-converged time-evolution operator—note that truncation may never increase the norm, but an ill-converged $U(\delta t)$ may both increase or decrease it. Changes in the total energy can also result from either of these, although in this case, the truncation may also increase the energy. The errors accumulated per timestep in these quantities are shown in Fig. 5. If not stated otherwise, the *paces* calculations shown here use $\delta t = 0.05/\omega$ and a nominal truncation number of 13×10^6 .

Qualitatively, there is good agreement between the results, but discrepancies between the results increase with increasing time t and increasing exciton–phonon strength g up to a few single-digit percentage points. Both of these aspects are unsurprising, as the wavefunction spreads out as t increases, and larger g causes higher-lying phonon-number states to become occupied, thereby also increasing spreading in the phononic Hilbert space and worsening compression artifacts. Furthermore, we see that the truncation error due to Q is around nine orders of magnitude higher than the error that is attributable to the finite-sum representation of $U(\delta t)$, which, as previously mentioned, is to be expected as the series expansion is continued until convergence is reached according to a ℓ^∞ criterion.

With regards to convergence as a function of the truncation cutoff number q , we see in Fig. 6 that, as expected,

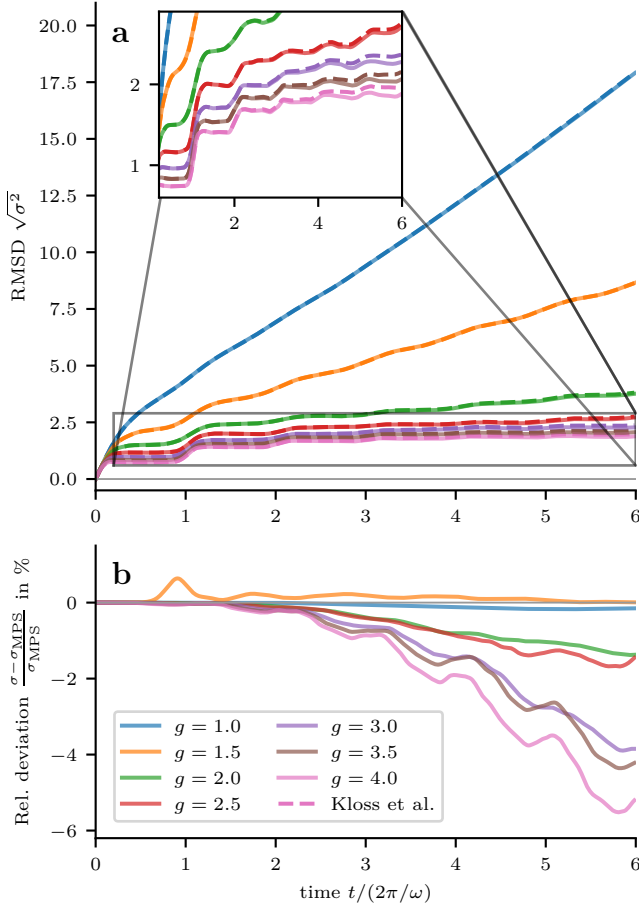


FIG. 4. A comparison between the RMSD values obtained using *paces* and those of Kloss et al.⁷¹ (compare to Fig. 2 therein). The initial state is a completely localized Franck-Condon-type excitation. **a**: *paces* (solid) and MPS⁷¹ results (dashed) for the RMSD (10). **b**: Relative deviations between the RMSD of the two methods.

the errors incurred by the calculation decrease with increasing q . Furthermore, the decay of the errors in the norm seems to match a power law with $\varepsilon(Q) \propto q^{-0.52}$ quite well, suggesting that in this situation and according to (8), the wavefunction coefficients may be distributed approximately as $|\langle n|\psi\rangle|^2 \propto n^{-2}$ —assuming we can extrapolate from the single-step error analysis performed above to a compounded error. This power law is also indicated in Fig. 2, and we see that the true distribution does not exactly match the estimated power law, but does roughly resemble it. Fig. 6 also reveals that the runtime scales remarkably linearly as a function of the nominal truncation parameter.

Finally, we remark that due to the high degree of parallelization, the present method is quite fast: For the strong coupling case of $g = 4\hbar\omega$, $J = \hbar\omega$, $L = 25$ and $\nu_{\text{max}} = 128$ (corresponding to a total Hilbert space dimension of over 10^{54}) up to $t = 40/\omega$, Kloss et al. report a total runtime of 156 hours⁷³, whereas the present

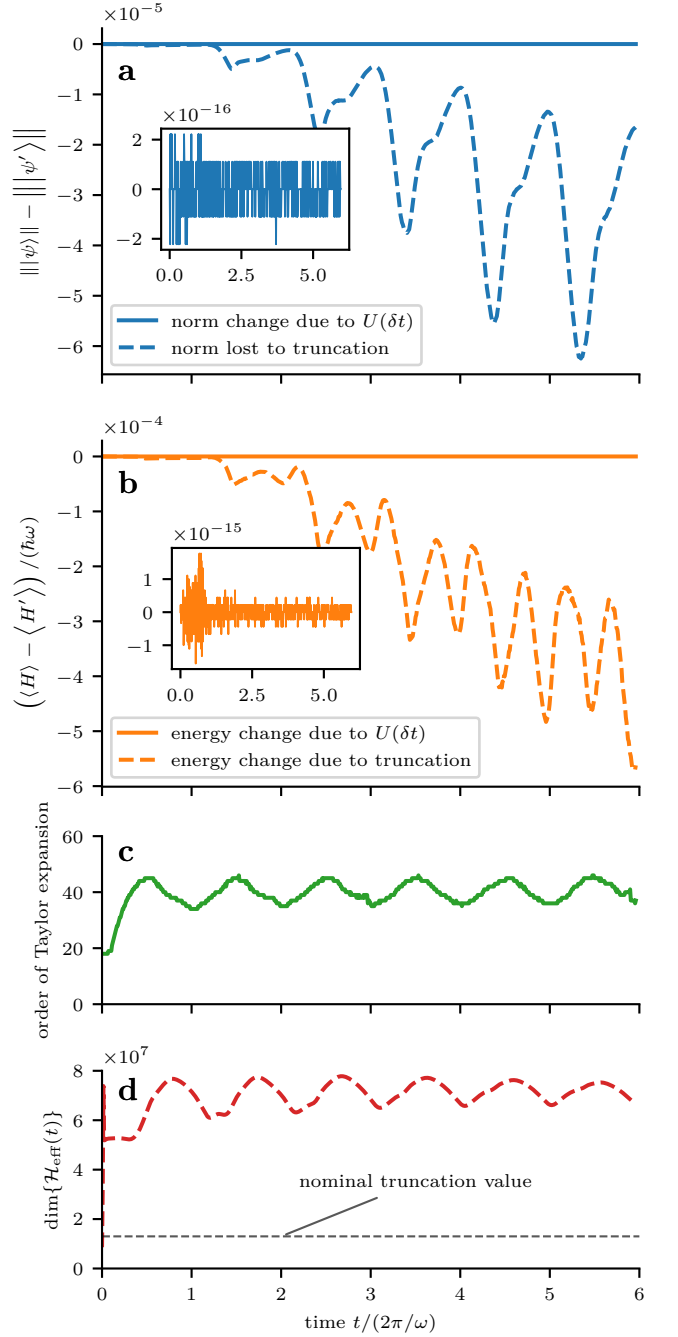


FIG. 5. Errors accumulated per timestep and convergence parameters from the $g = 4$ simulation of Fig. 4. **a**: Norm loss *per timestep* due to the truncation of the series expansion of $U(\delta t)$ and the truncation Q of the state vector $|\psi(t)\rangle$. Insets show a zoom on the $U(\delta t)$ truncation error, which is negligibly small due to its adaptive termination after reaching a set convergence criterion. **b**: Same as **b**, but for the change in energy per timestep. **c**: The order of the expansion of $U(\delta t)$ that was required for convergence. **d**: The dimension of the effective Hilbert space, which expands and contracts depending on the structure of $|\psi(t)\rangle$. Dashed line is the nominal truncation value 13×10^6 , prior to the post-adaptation detruncation of section III B 4.

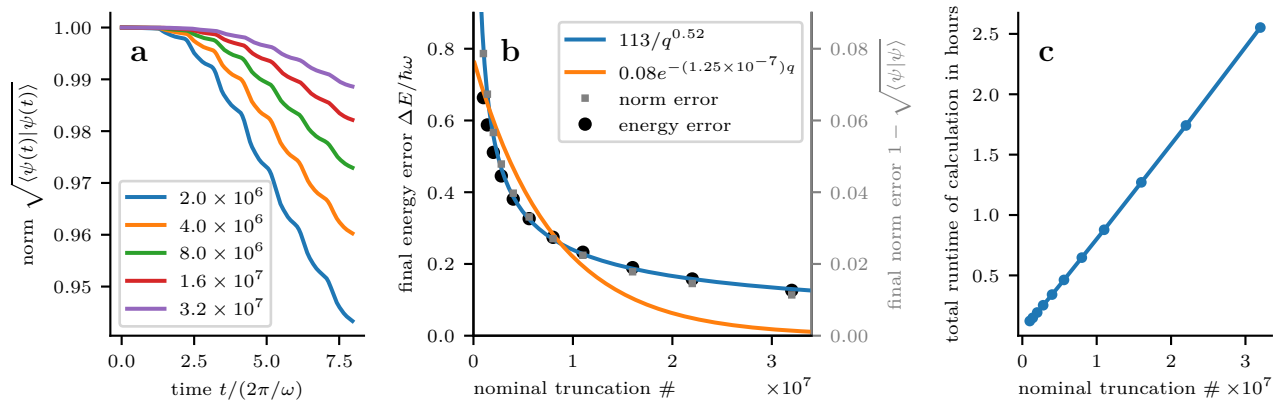


FIG. 6. Convergence as a function of the nominal truncation number: Note that this nominal number is smaller than the “true” dimension q given by the projection Q due to the detruncation procedure of section III B 4. The quantities used to gauge convergence here are the norm $\sqrt{\langle \psi | \psi \rangle}$ and the average total energy $\langle H \rangle$, which should both be conserved in an exact calculation. Apart from q , the calculations shown here are identical to Fig. 5. **a:** The time evolution of the norm for representative calculations with different nominal truncation numbers. **b:** The deviation from the exact value in terms of the total energy (black circles) and the norm (gray squares) at the end of the calculation at $t = 8 \frac{2\pi}{\omega}$, along with least-squares fit of the error in the norm based on a power law (blue) or an exponential decay (orange). **c:** The total runtime of the calculation as a function of q . Runtime given here is for one Nvidia A100 (80 GiB HBM2e) per run.

parallelized method required 90 minutes for the same calculation⁷⁴, though a more thorough investigation of runtime comparisons across a wider range of hardware configurations would be warranted.

VI. CONCLUSION & OUTLOOK

We have presented a parallelized, efficient method for computing quantum dynamics of pure states based on physically motivated co-evolving subspaces. The method is, in principle, applicable to any system in which the basis admits a sparse representation of both the Hamiltonian and the initial state, and will work effectively as long as the state remains relatively sparse in the Hilbert space. We have compared its merits and weaknesses to other existing methods and identified said basis representation as a crucial element in its effectiveness, whereas high dimensionality (both geometrically and in terms of the Hilbert space) or entanglement are peripheral to its applicability.

We would like to highlight two interesting obvious extensions of the method: First, the method is readily extensible to time-dependent Hamiltonians that satisfy the above criteria, as long as Trotterization along the time axis is an acceptable approximation. In other words, if a time-dependent Hamiltonian can be well-approximated as a piecewise constant-in-time Hamiltonian, then the method trivially extends to such a system by simply adjusting the Hamiltonian accordingly at each timestep. Particularly well-suited time-dependent Hamiltonians include those that exhibit changes only in the magnitude of their coupling and not in their graph structure, e.g., time-dependent driving of an otherwise constant operator such as $\cos(\omega t)\sigma_x$, etc., a simple albeit ubiquitous

form of time-dependent Hamiltonian.

Second, open quantum systems dynamics are also accessible: In the simplest case, by vectorizing a master equation and effectively replacing the Hamiltonian by the Lindblad or Redfield generator. The spread of the vector would then represent spreading of populations and coherences rather than basis states in the Hilbert space. This provides direct access to the perturbative system–bath coupling regime⁷⁵, but can also be combined with existing techniques such as pseudomodes^{76,77} or chain mappings^{78,79} to access the non-Markovian, non-perturbative regime in a controlled manner. Furthermore, using techniques such as T-TEDOPA^{80,81} or quantum jumps^{82,83}, even the current wavefunction-based approach may be amenable to treating open quantum systems efficiently, which could then, for example, be further extended using the transfer-tensor method^{84,85}.

ACKNOWLEDGMENTS

I am indebted to Martin Plenio and Susana Huelga for their support, supervision and many valuable discussions, and to Salvatore Manmana for his tireless enthusiasm, encouragement and truly in-depth discussions on this project. I am especially grateful to Jianshu Cao for hosting me in his group and for the inspiring and supportive environment he provided during the development of this work. I also thank the many colleagues who provided feedback and insightful discussions on this manuscript and its underlying ideas, in particular Gabriela Wójtowicz, Thibaut Lacroix, Nicola Lorenzoni and Carlos Munuera Javaloy. Furthermore, I would like to thank Benedikt Kloss for providing access to the data used in Fig. 4.

I acknowledge generous scholarships and travel funds provided by the *Studienstiftung des deutschen Volkes*, as well as funding provided by: the German Research Foundation (DFG) – 217133147/SFB 1073, project B03, the German Federal Ministry of Science (BMFTR) under the project SPINNING (Grant No. 13NI6215), and the BMFTR project PhoQuant (Grant No. 13N16110). I also gratefully acknowledge computational resources provided by the state of Baden-Württemberg through bwHPC and the DFG through Grant No. INST 40/575-1 FUGG (JUSTUS 2 cluster) and GPU resources provided by the Institute of Theoretical Physics in Göttingen and financed by the DFG and the Bundesministerium für Bildung und Forschung (BMBF).

AUTHOR DECLARATIONS

The author has no conflicts to disclose.

DATA AVAILABILITY

The data that support the findings of this study are available from the corresponding author upon reasonable request. The code (which makes extensive use of CuPy⁸⁶) that was used to generate the data presented in this study is publicly available in the `holstein_only` branch of <https://github.com/rkevk/paces>.

- ¹I. V. Oseledets and E. E. Tyrtyshnikov, “Breaking the curse of dimensionality, or how to use SVD in many dimensions,” *SIAM Journal on Scientific Computing* **31**, 3744–3759 (2009).
- ²H. Wang, “Multilayer multiconfiguration time-dependent hartree theory,” *The Journal of Physical Chemistry A* **119**, 7951–7965 (2015).
- ³R. Borrelli and M. F. Gelin, “Quantum electron-vibrational dynamics at finite temperature: Thermo field dynamics approach,” *The Journal of Chemical Physics* **145**, 224101 (2016).
- ⁴X. Xie, Y. Liu, Y. Yao, U. Schollwöck, C. Liu, and H. Ma, “Time-dependent density matrix renormalization group quantum dynamics for realistic chemical systems,” *The Journal of Chemical Physics* **151**, 224101 (2019).
- ⁵A. Palacios, H. Bachau, and F. Martín, “Enhancement and control of H₂ dissociative ionization by femtosecond VUV laser pulses,” *Phys. Rev. Lett.* **96**, 143001 (2006).
- ⁶R. K. Kessing, P.-Y. Yang, S. R. Manmana, and J. Cao, “Long-range nonequilibrium coherent tunneling induced by fractional vibronic resonances,” *The Journal of Physical Chemistry Letters* **13**, 6831–6838 (2022).
- ⁷S. R. White, “Density matrix formulation for quantum renormalization groups,” *Phys. Rev. Lett.* **69**, 2863–2866 (1992).
- ⁸S. R. White and R. M. Noack, “Real-space quantum renormalization groups,” *Phys. Rev. Lett.* **68**, 3487–3490 (1992).
- ⁹S. R. White, “Density-matrix algorithms for quantum renormalization groups,” *Phys. Rev. B* **48**, 10345–10356 (1993).
- ¹⁰K. G. Wilson, “The renormalization group: Critical phenomena and the Kondo problem,” *Rev. Mod. Phys.* **47**, 773–840 (1975).
- ¹¹J. C. Bridgeman and C. T. Chubb, “Hand-waving and interpretive dance: an introductory course on tensor networks,” *Journal of Physics A: Mathematical and Theoretical* **50**, 223001 (2017).
- ¹²U. Schollwöck, “The density-matrix renormalization group in the age of matrix product states,” *Annals of Physics* **326**, 96 – 192 (2011), january 2011 Special Issue.
- ¹³S. Paeckel, T. Köhler, A. Swoboda, S. R. Manmana, U. Schollwöck, and C. Hubig, “Time-evolution methods for matrix-product states,” *Annals of Physics* **411**, 167998 (2019).
- ¹⁴F. Verstraete and J. I. Cirac, “Matrix product states represent ground states faithfully,” *Phys. Rev. B* **73**, 094423 (2006).
- ¹⁵T. Lacroix, “Influence of the ordering of the chains modes,” in *Beyond Markovian Dissipation at the Nanoscale: Towards Quantum Design Rules for Bio-organic Nanodevices* (Springer Nature Switzerland, Cham, 2025) Chap. 5, pp. 77–93.
- ¹⁶T. Lacroix, B. W. Lovett, and A. W. Chin, “Connectivity matters: Impact of bath modes ordering and geometry in open quantum system simulation with tensor network states,” (2025), [arXiv:2409.04145 \[quant-ph\]](https://arxiv.org/abs/2409.04145).
- ¹⁷C. Zhang, E. Jeckelmann, and S. R. White, “Density matrix approach to local Hilbert space reduction,” *Phys. Rev. Lett.* **80**, 2661–2664 (1998).
- ¹⁸C. Zhang, E. Jeckelmann, and S. R. White, “Dynamical properties of the one-dimensional Holstein model,” *Phys. Rev. B* **60**, 14092–14104 (1999).
- ¹⁹C. Brockt, F. Dorfner, L. Vidmar, F. Heidrich-Meisner, and E. Jeckelmann, “Matrix-product-state method with a dynamical local basis optimization for bosonic systems out of equilibrium,” *Phys. Rev. B* **92**, 241106 (2015).
- ²⁰F. A. Y. N. Schröder and A. W. Chin, “Simulating open quantum dynamics with time-dependent variational matrix product states: Towards microscopic correlation of environment dynamics and reduced system evolution,” *Phys. Rev. B* **93**, 075105 (2016).
- ²¹D. V. Shalashilin and M. S. Child, “Time dependent quantum propagation in phase space,” *The Journal of Chemical Physics* **113**, 10028–10036 (2000).
- ²²D. V. Shalashilin and M. S. Child, “Real time quantum propagation on a monte carlo trajectory guided grids of coupled coherent states: 26D simulation of pyrazine absorption spectrum,” *The Journal of Chemical Physics* **121**, 3563–3568 (2004).
- ²³M. Ben-Nun, J. Quenneville, and T. J. Martínez, “Ab initio multiple spawning: photochemistry from first principles quantum molecular dynamics,” *The Journal of Physical Chemistry A* **104**, 5161–5175 (2000).
- ²⁴B. Gu and S. Garashchuk, “Quantum dynamics with Gaussian bases defined by the quantum trajectories,” *The Journal of Physical Chemistry A* **120**, 3023–3031 (2016).
- ²⁵M. Werther and F. Großmann, “Apoptosis of moving nonorthogonal basis functions in many-particle quantum dynamics,” *Phys. Rev. B* **101**, 174315 (2020).
- ²⁶L. R. Petthey and R. E. Wyatt, “Wave packet dynamics with adaptive grids: The moving boundary truncation method,” *Chemical Physics Letters* **424**, 443 – 448 (2006).
- ²⁷L. R. Petthey and R. E. Wyatt, “Quantum wave packet dynamics on multidimensional adaptive grids: Applications of the moving boundary truncation method,” *International Journal of Quantum Chemistry* **107**, 1566–1573 (2007).
- ²⁸Y. Wu and V. S. Batista, “Matching-pursuit for simulations of quantum processes,” *The Journal of Chemical Physics* **118**, 6720–6724 (2003).
- ²⁹Y. Wu and V. S. Batista, “Quantum tunneling dynamics in multidimensional systems: A matching-pursuit description,” *The Journal of Chemical Physics* **121**, 1676–1680 (2004).
- ³⁰X. Chen and V. S. Batista, “Matching-pursuit/split-operator-Fourier-transform simulations of excited-state nonadiabatic quantum dynamics in pyrazine,” *The Journal of Chemical Physics* **125**, 124313 (2006).
- ³¹W. Koch and T. J. Frankcombe, “Basis expansion leaping: A new method to solve the time-dependent schrödinger equation for molecular quantum dynamics,” *Phys. Rev. Lett.* **110**, 263202 (2013).
- ³²M. A. C. Saller and S. Habershon, “Quantum dynamics with short-time trajectories and minimal adaptive basis sets,” *Journal of Chemical Theory and Computation* **13**, 3085–3096 (2017).
- ³³G. Richings, I. Polyak, K. Spinlove, G. Worth, I. Burghardt, and B. Lasorne, “Quantum dynamics simulations using Gaus-

- sian wavepackets: the vMCG method,” *International Reviews in Physical Chemistry* **34**, 269–308 (2015).
- ³⁴B. Hartke, “Propagation with distributed Gaussians as a sparse, adaptive basis for higher-dimensional quantum dynamics,” *Phys. Chem. Chem. Phys.* **8**, 3627–3635 (2006).
- ³⁵J. Sielk, H. F. von Horsten, F. Krüger, R. Schneider, and B. Hartke, “Quantum-mechanical wavepacket propagation in a sparse, adaptive basis of interpolating Gaussians with collocation,” *Phys. Chem. Chem. Phys.* **11**, 463–475 (2009).
- ³⁶J. Bonča, S. A. Trugman, and I. Batistić, “Holstein polaron,” *Phys. Rev. B* **60**, 1633–1642 (1999).
- ³⁷J. Bonča, T. Katrašnik, and S. A. Trugman, “Mobile bipolaron,” *Phys. Rev. Lett.* **84**, 3153–3156 (2000).
- ³⁸L.-C. Ku, S. A. Trugman, and J. Bonča, “Dimensionality effects on the holstein polaron,” *Phys. Rev. B* **65**, 174306 (2002).
- ³⁹J. Bonča, S. Maekawa, T. Tohyama, and P. Prelovšek, “Spectral properties of a hole coupled to optical phonons in the generalized $t-j$ model,” *Phys. Rev. B* **77**, 054519 (2008).
- ⁴⁰L. Vidmar, J. Bonča, S. Maekawa, and T. Tohyama, “Bipolaron in the $t-j$ model coupled to longitudinal and transverse quantum lattice vibrations,” *Phys. Rev. Lett.* **103**, 186401 (2009).
- ⁴¹L. Vidmar, J. Bonča, M. Mierzejewski, P. Prelovšek, and S. A. Trugman, “Nonequilibrium dynamics of the holstein polaron driven by an external electric field,” *Phys. Rev. B* **83**, 134301 (2011).
- ⁴²L. Vidmar, J. Bonča, T. Tohyama, and S. Maekawa, “Quantum dynamics of a driven correlated system coupled to phonons,” *Phys. Rev. Lett.* **107**, 246404 (2011).
- ⁴³D. Golež, J. Bonča, L. Vidmar, and S. A. Trugman, “Relaxation dynamics of the holstein polaron,” *Phys. Rev. Lett.* **109**, 236402 (2012).
- ⁴⁴M. Chakraborty and B. I. Min, “Self-consistent basis generation scheme for polaron and bipolaron systems,” *Phys. Rev. B* **88**, 024302 (2013).
- ⁴⁵L. Vidmar and J. Bonča, “Two holes in the $t-j$ model form a bound state for any nonzero j/t ,” *Journal of Superconductivity and Novel Magnetism* **26**, 2641–2645 (2013).
- ⁴⁶F. Dorfner, L. Vidmar, C. Brockt, E. Jeckelmann, and F. Heidrich-Meisner, “Real-time decay of a highly excited charge carrier in the one-dimensional Holstein model,” *Phys. Rev. B* **91**, 104302 (2015).
- ⁴⁷S. R. Manmana, A. Muramatsu, and R. M. Noack, “Time evolution of one-dimensional quantum many body systems,” *AIP Conference Proceedings* **789**, 269–278 (2005).
- ⁴⁸D. Poulin, A. Qarry, R. Somma, and F. Verstraete, “Quantum simulation of time-dependent Hamiltonians and the convenient illusion of Hilbert space,” *Phys. Rev. Lett.* **106**, 170501 (2011).
- ⁴⁹F. Verstraete, V. Murg, and J. Cirac, “Matrix product states, projected entangled pair states, and variational renormalization group methods for quantum spin systems,” *Advances in Physics* **57**, 143–224 (2008).
- ⁵⁰M. Steinberger, A. Derlery, R. Zayer, and H. Seidel, “How naive is naive SpMV on the GPU?” in *2016 IEEE High Performance Extreme Computing Conference (HPEC)* (2016) pp. 1–8.
- ⁵¹A. H. Al-Mohy and N. J. Higham, “Computing the action of the matrix exponential, with an application to exponential integrators,” *SIAM Journal on Scientific Computing* **33**, 488–511 (2011).
- ⁵²E. Farhi and S. Gutmann, “Quantum computation and decision trees,” *Phys. Rev. A* **58**, 915–928 (1998).
- ⁵³S. Roy and A. Lazarides, “Strong ergodicity breaking due to local constraints in a quantum system,” *Phys. Rev. Res.* **2**, 023159 (2020).
- ⁵⁴J.-Y. Desautels, K. Bull, A. Daniel, and Z. Papić, “Hypergrid subgraphs and the origin of scarred quantum walks in many-body Hilbert space,” *Phys. Rev. B* **105**, 245137 (2022).
- ⁵⁵H. G. Menzler, M. C. Bañuls, and F. Heidrich-Meisner, “Graph theory and tunable slow dynamics in quantum East Hamiltonians,” *Phys. Rev. B* **112**, 115141 (2025).
- ⁵⁶S. Singh, R. N. C. Pfeifer, and G. Vidal, “Tensor network decompositions in the presence of a global symmetry,” *Phys. Rev. A* **82**, 050301 (2010).
- ⁵⁷S. Paeckel, T. Köhler, and S. R. Manmana, “Automated construction of $U(1)$ -invariant matrix-product operators from graph representations,” *SciPost Phys.* **3**, 035 (2017).
- ⁵⁸M. M. Rams, G. Wójtowicz, A. Sinha, and J. Hasik, “YASTN: Yet another symmetric tensor networks; A Python library for Abelian symmetric tensor network calculations,” *SciPost Phys. Codebases*, 52 (2025).
- ⁵⁹A. Krylov, “De la résolution numérique de l’équation servant à déterminer dans des questions de mécanique appliquée les fréquences de petites oscillations des systèmes matériels,” *Bulletin de l’Académie des Sciences de l’URSS. Classe des sciences mathématiques et na*, 491–539 (1931).
- ⁶⁰Y. Saad, “Krylov subspace methods, part I,” in *Iterative Methods for Sparse Linear Systems* (Society for Industrial and Applied Mathematics., 2003) Chap. 6, pp. 151–216, 2nd ed.
- ⁶¹W. Li, J. Ren, and Z. Shuai, “Numerical assessment for accuracy and GPU acceleration of TD-DMRG time evolution schemes,” *The Journal of Chemical Physics* **152**, 024127 (2020).
- ⁶²D. I. Lyakh, T. Nguyen, D. Claudino, E. Dumitrescu, and A. J. McCaskey, “Exatn: Scalable gpu-accelerated high-performance processing of general tensor networks at exascale,” *Frontiers in Applied Mathematics and Statistics Volume 8 - 2022* (2022), 10.3389/fams.2022.838601.
- ⁶³F. Pan and P. Zhang, “Simulation of quantum circuits using the big-batch tensor network method,” *Phys. Rev. Lett.* **128**, 030501 (2022).
- ⁶⁴A. Menczer and Ö. Legeza, “Massively parallel tensor network state algorithms on hybrid cpu-gpu based architectures,” *Journal of Chemical Theory and Computation* **21**, 1572–1587 (2025).
- ⁶⁵M. A. Bender, G. S. Brodal, R. Fagerberg, R. Jacob, and E. Vicari, “Optimal sparse matrix dense vector multiplication in the I/O-model,” *Theory of Computing Systems* **47**, 934–962 (2010).
- ⁶⁶J. Eisert, M. Cramer, and M. B. Plenio, “Colloquium: Area laws for the entanglement entropy,” *Rev. Mod. Phys.* **82**, 277–306 (2010).
- ⁶⁷F. Mintert, C. Viviescas, and A. Buchleitner, “Basic concepts of entangled states,” in *Entanglement and Decoherence: Foundations and Modern Trends*, edited by A. Buchleitner, C. Viviescas, and M. Tiersch (Springer Berlin Heidelberg, Berlin, Heidelberg, 2009) Chap. 2, pp. 61–86.
- ⁶⁸I. G. Lang and Y. A. Firsov, “Kinetic Theory of Semiconductors with Low Mobility,” *Soviet Journal of Experimental and Theoretical Physics* **16**, 1301 (1963).
- ⁶⁹D. Xu and J. Cao, “Non-canonical distribution and non-equilibrium transport beyond weak system-bath coupling regime: A polaron transformation approach,” *Frontiers of Physics* **11**, 110308 (2016).
- ⁷⁰A. H. Al-Mohy and N. J. Higham, “A new scaling and squaring algorithm for the matrix exponential,” *SIAM Journal on Matrix Analysis and Applications* **31**, 970–989 (2010).
- ⁷¹B. Kloss, D. R. Reichman, and R. Tempelaar, “Multiset matrix product state calculations reveal mobile Franck-Condon excitations under strong Holstein-type coupling,” *Phys. Rev. Lett.* **123**, 126601 (2019).
- ⁷²Reference 71 refers to electrons, but since we are considering only a single particle, this is, for the purposes of the Holstein Hamiltonian, equivalent to a single exciton.
- ⁷³Running as a single process on a Xeon E5-2690 v3 at 2.60 GHz, released in 2014.
- ⁷⁴On an Nvidia V100S (32 GiB HBM2), max. clock speed 1597 MHz, released in 2019.
- ⁷⁵A. Fruchtmann, N. Lambert, and E. M. Gauger, “When do perturbative approaches accurately capture the dynamics of complex quantum systems?” *Scientific Reports* **6**, 28204 (2016).
- ⁷⁶B. M. Garraway, “Nonperturbative decay of an atomic system in a cavity,” *Phys. Rev. A* **55**, 2290–2303 (1997).

- ⁷⁷D. Tamascelli, A. Smirne, S. F. Huelga, and M. B. Plenio, “Nonperturbative treatment of non-markovian dynamics of open quantum systems,” *Phys. Rev. Lett.* **120**, 030402 (2018).
- ⁷⁸J. Prior, A. W. Chin, S. F. Huelga, and M. B. Plenio, “Efficient simulation of strong system-environment interactions,” *Phys. Rev. Lett.* **105**, 050404 (2010).
- ⁷⁹A. W. Chin, . Rivas, S. F. Huelga, and M. B. Plenio, “Exact mapping between system-reservoir quantum models and semi-infinite discrete chains using orthogonal polynomials,” *Journal of Mathematical Physics* **51**, 092109 (2010).
- ⁸⁰D. Tamascelli, A. Smirne, J. Lim, S. F. Huelga, and M. B. Plenio, “Efficient simulation of finite-temperature open quantum systems,” *Phys. Rev. Lett.* **123**, 090402 (2019).
- ⁸¹B. Le Dé, A. Jaouadi, E. Mangaud, A. W. Chin, and M. Desouter-Lecomte, “Managing temperature in open quantum systems strongly coupled with structured environments,” *The Journal of Chemical Physics* **160**, 244102 (2024).
- ⁸²J. Dalibard, Y. Castin, and K. Mølmer, “Wave-function approach to dissipative processes in quantum optics,” *Phys. Rev. Lett.* **68**, 580–583 (1992).
- ⁸³M. B. Plenio and P. L. Knight, “The quantum-jump approach to dissipative dynamics in quantum optics,” *Rev. Mod. Phys.* **70**, 101–144 (1998).
- ⁸⁴J. Cerrillo and J. Cao, “Non-markovian dynamical maps: Numerical processing of open quantum trajectories,” *Phys. Rev. Lett.* **112**, 110401 (2014).
- ⁸⁵R. Rosenbach, J. Cerrillo, S. F. Huelga, J. Cao, and M. B. Plenio, “Efficient simulation of non-markovian system-environment interaction,” *New Journal of Physics* **18**, 023035 (2016).
- ⁸⁶R. Okuta, Y. Unno, D. Nishino, S. Hido, and C. Loomis, “Cupy: A NumPy-compatible library for NVIDIA GPU calculations,” in *Proceedings of Workshop on Machine Learning Systems (LearningSys) in The Thirty-first Annual Conference on Neural Information Processing Systems (NIPS)* (2017).
- ⁸⁷R. M. Noack and S. R. Manmana, “Diagonalization- and numerical renormalization-group-based methods for interacting quantum systems,” *AIP Conference Proceedings* **789**, 93–163 (2005).

Appendix A: Series-based exponentiation compared to a Lanczos algorithm

As briefly discussed in section III A, the main allure of the computation of $e^A v$ via repeated application of $\frac{A}{n}$ to v is that it is $\mathcal{O}(1)$ in space, i.e., independent of the order of the expansion. Calculating the series expansion up to order m is $\mathcal{O}(m)$ in time, however, due to the existence of highly efficient parallelized algorithms for this comparatively simple SpMV application, the linear scaling in time has a very small prefactor, and instead memory is *the* limiting factor for the entire method. Therefore, the constant memory requirement vastly outweighs the potential downsides of linear scaling in time.

On the other hand, one could apply a Lanczos decomposition to compute a single time evolution step as⁸⁷

$$e^{-i\delta t H/\hbar} |\psi(t)\rangle \approx V_n e^{-i\delta t T_n/\hbar} V_n^\dagger |\psi(t)\rangle,$$

where V_n is a $(\dim\{\mathcal{H}\} \times n)$ matrix that maps from the Krylov space K^n to the Hilbert space, and V_n^\dagger is its adjoint. T_n is the tridiagonal $(n \times n)$ matrix resulting from the Lanczos procedure, similar to a partial diagonalization of H within K^n . This method and its application to MPS are discussed under the name “global Krylov method” in ref. 13.

The transformation into Krylov subspaces typically requires only relatively low dimensions on the order of 10 to 30, smaller than the number of iterations we use for the Taylor expansion (see Fig. 5c). However, the Krylov method is computationally slightly more demanding than the series-based method: The generation of n Lanczos vectors also naturally requires m applications of H onto a vector, as well as orthogonalization via the calculation of inner products and ℓ^2 norms, which both require more computational time. The main issue, however, is that the construction of the V_n matrix, which is composed of n dense vectors each of the same dimension as the total Hilbert space, is very memory-intensive—and of order $\mathcal{O}(n)$ in both time *and* memory, unlike the $\mathcal{O}(1)$ memory behavior of the series-expansion method. This is ultimately the greatest benefit of the expansion method over the Lanczos method, since on GPUs, highly parallelized applications of SpMV operations are cheap while memory is not.

To illustrate this point, we shall insert some numbers. Assume we have 16 GiB of GPU RAM at our disposal, of which we would like to allocate at most $\frac{1}{4}$ to V_n to leave sufficient headroom for the remaining matrices, vectors, etc. Given that the effective size of the Hilbert space in simulations that were run on these GPUs was around 7×10^7 , each 128-bit complex-valued vector requires approximately 1 GiB. If we were to construct a V_n with a relatively modest $n = 20$, then this V_n alone would consume over 20 GiB in memory, already exceeding the total amount of available memory without any regard to other matrices, vectors, etc. By contrast, the only additional memory requirements of the series expansion method in this situation is that of a single temporary vector, i.e., 1 GiB, as discussed in section III A.